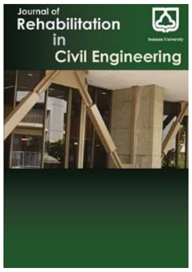

journal homepage: http://civiljournal.semnan.ac.ir/

Torsion Effect on the RC Structures using Fragility Curves Considering with Soil-Structure Interaction

A. Anvarsamarin[1], F. Rahimzadeh Rofooei[2*] and M. Nekooei[1]

1. Department of civil Engineering, Science and Research Branch, Islamic Azad University, Tehran, Iran
2. Civil Engineering Department, Sharif University of Technology, Tehran, Iran

Corresponding author: rofooei@sharif.edu

ARTICLE INFO

Article history:
Received: 2 October 2018
Accepted: 15 February 2019

Keywords:
Intensity Measure,
Collapse Fragility Curve,
Incremental Dynamic Analysis,
Intensity Measure,
Mass Center Eccentricity,
Soil-Structure Interaction.

ABSTRACT

The existence of torsion, as well as consideration of the Soil-Structure Interaction (SSI), increase the natural periods of the structure resulting from a subsequent decrease in the seismic demand of the system. This paper summarizes the probabilistic assessment in order to evaluate the collapse fragility curves in concrete moment resisting structure with different mass center eccentricities. A 12-story, 3-D, moment resisting concrete structure with fixed-base and deliberating SSI, both types of one- and two-way eccentricities is employed to estimate the collapse fragility curve by the IM-based approach. In consonance with the obtained results, increasing the torsion as a result of shifting the mass centers decreases the median of the collapse fragility curve. In addition, it was observed that the SSI consideration for soil type D with shear wave velocity of 180m/s to 360m/s leads to reduction of the median of collapse capacity by 30%−40% in the presence of torsion effect due to one- and two-way mass center eccentricities in range of 0-20% of the building's plan dimensions respectively. Put it differently, the fixed-base assumption overestimates the median of collapse capacity and leads to unsafe design. Moreover, shifting the mass centers of all the stories up to 20% of the building's plan dimensions, with or without the consideration of the SSI, decreases the median of collapse capacities and increases the seismic vulnerability of the building. Accordingly, the fixed-base assumption can be underestimated the dispersion range of the collapse fragility curve. The result reveals that the mentioned differences cannot be neglected.

1. Introduction

The study of the global collapse was triggered by considering P-Δ effects on seismic response. Although hysteresis models contemplated positive post-yielding stiffness, the structure tangent stiffness became negative under large P-Δ effects which in

DOI: 10.22075/JRCE.2019.16080.1302

turn lead to the structural collapse. Seismic demands exceeding the tolerable limits of a structure reduce the strength and stiffness of structural elements and this may result in global or partial collapse of the building. Structural performance assessment requires a numerical criterion. Confirming to FEMA 2000, the Incremental Dynamic Analysis (IDA) approach is proposed to estimate the structural capacity of the buildings. In addition, FEMA 2000 is classified the point of occurrence of collapse based on the following conditions: Numerical non-convergence in Structural analysis algorithm, The occurrence of a slope equal to 20% of the initial elastic slope in the IDA curve and Exceedance of the maximum internal drift ratio (IDR) above %10. Jalayer and Cornell used the IDA concept to estimate the total dynamic instability capacity of a regular RC structure. The study deliberated strength deterioration caused by the shear failure of columns in accordance with the model developed by Pincheria in 1999 [1]. The stochastic nature of strong ground motions and the fact that no analytical approach can model all features of structural behavior increase the complexity of the seismic collapse analysis of structures [2-5]. A performance target in collapse level can be considered as a tolerable collapse probability in a given hazard level.

Currently, the collapse fragility curve is the major and accepted tool for evaluating the collapse of the structure. A set of IDA analyses can play a vital role in determining the estimation parameters and in turn determine the collapse fragility curve. Incremental Dynamic Analysis (IDA) was invented to take the inherent variability of earthquakes into account during the seismic response analysis of structures [6]. The probabilistic estimation of maximum story drift demands by deliberating a nine-story, moment resisting frame building exposed to a set of 40 ground motions was ameliorated by Stoica et al. [7]. Vulnerability assessment methodology has been developed by Andreas J. Kappos and Georgios Panagopoulos to estimate the fragility curves of all types of common RC buildings in Greece. This methodology was in consonance with the hybrid approach, which combines statistical data with properly processed results from nonlinear static or dynamic analyses. This procedure permit interpolation and (under certain conditions) extrapolation of statistical data to PGAs and/or spectral displacements for which no data is available [8]. Haselton and Dierlin evaluated the collapse risk of 30 four-story buildings with a special moment frame designed in accordance with ASCE9-02. According to their results, the likelihood of structural collapse for earthquakes with a return period of 2475 years ranges from 3% to 20% with a mean of 11% [9]. Lignos et al. applied the results of a collapse test conducted on a 4-story steel moment frame on the shaking table of the E-Defence laboratory and derived the essential parameters required for modeling the collapse reliability of buildings. They concluded that Riley damping causes better results than stiffness-proportional damping. Moreover, they showed that the accurate estimation of the collapse capacities of structures demands the consideration of P-Δ effects [10]. Palermo et al. evaluated the efficiency of current modeling techniques in predicting the collapse capacity of the studied structures. According to the study, modern techniques have a better capability of predicting the collapse capacity of structures [11].

During the past three decades, extensive researches have been focused on the Soil-

Structure Interaction (SSI) effect on structural performance, especially strategic ones [12]. Even though several codes such as ATC-3-06, NEHRP-2012, and NIST GCR 12-917-21 do not extend the interest on SSI effects to residential buildings [13-15]. This is due to the numerical simulation challenges of the SSI effect. In particular, many simplifications are considered in finite element models for residential structures, e.g., the study performed by Renzi et al. [16]. Therefore, these approaches should be verified in order to correctly assess the SSI effect. Some researchers have modeled the effect of soil-structure interaction with direct method [17- 21]. In addition, there are cases that modeled the soil with different approaches such as beam-on-nonlinear-Winkler-foundation [22, 23], elasto-plastic Mohr-Coulomb modeling [24] and equivalent linear behaviors [25, 26]. The seismic performance and energy dissipation of structures can significantly be changed through contemplating the SSI effects. Khoshnoudian et al. showed that soil flexibility increases the dynamic instability of the structural system, and collapse strength reduction factor highly decreases by increasing non-dimensional frequency [23].

Recently, Shakib and Homaei demonstrated that SSI consideration reduces the structural seismic capacities, ductile deformation and life-safety confidence level [27]. Moreover, it was revealed that by taking into account SSI, it increases the drift demand and causes that the location of maximum drift moves to the first story [28]. They showed that SSI changes the pattern of distribution of vulnerability, especially for the beams of shear wall buildings, and increases the seismic vulnerability on soft soils. Also, Ghandil et al. applied the direct method by deliberating a nonlinear behavior for the frame elements of the structure in order to demonstrate that SSI increases the drifts and ductility demands of the lower stories [29]. SSI effect on fragility curves of RC moment resisting frame buildings inspected by applying the direct method [30]. The evaluation of the seismic fragility curve of the structure is a prerequisite for seismic loss estimation and risk management. The seismic vulnerability of structures is usually expressed by a fragility function, which indicates the probability of exceeding prescribed levels of damage for a wide range of ground motion intensities. Currently, available seismic fragility databases for RC buildings [31] are developed for fixed based structures ignoring SSI effect.

Assessing the seismic performance of structures during the past earthquakes indicates that irregularities due to mass, stiffness, and distribution of strength are one of the main reasons for the vulnerability of the structures. The existence of torsion in buildings causes changes in the seismic demands in the different corner of each story, so under severe ground motion, some members of the frame on the side of the building may experience non-linear behavior while the frame members on the other side of the building are still in the elastic region. Torsion and soil-structure Interaction (SSI) can alter the performance of structure totally including its dynamic characteristics, response maxima and more important, distribution of nonlinear response through the structure where the accurate calculation of it is vital for the performance evaluation. This paper aims to move from the previous contributions to extend the assessment of the SSI effect on different mass center eccentricities, considering both types of the one- and two-way eccentricities.

This study employs 12-story moment resisting RC building to estimate the effect of torsion and soil-structure interaction (SSI) consideration on the median and dispersion of the collapse fragility curves. In order to evaluate the effect of torsion in both types of the fixed- and flexible-base of the building, the mass centers of all the stories was shifted as much as 0 to 20% of the building's plan dimensions subjected to the simultaneous effects of the horizontal components of the selected earthquake records.

2. Case Study and Numerical Modeling

2.1. Design Characteristics

A 12-story building with 3-D moment resisting frame RC structure with a fundamental period of 1.375 seconds was considered and designed confirming to the ACI 318-08 and ASCE 7-10 code requirements [32, 33]. This structural model is assumed to be of administrative buildings type with the same plan dimensions, located in a high seismic site at California with site class D according to the ASCE 7-10 [33]. The seismic parameters Ss and S_1 were considered 1.4438 and 0.612, respectively; the importance factor (I) of 1, the response modification factor (R) of 5 were considered, and the seismic coefficient (Cs) of 0.089 based on ASCE 7-10 [33]. The structural system of the 12-story building is an intermediate moment resisting frame. The specified compressive strength of concrete is 240 kg/cm^2. In all members, the ultimate strength of longitudinal bars is 5000 kg/cm2. The ETABS (2013) program was applied to design the structural models [34]. The studied building has a 30 m×18 m rectangle plan with a story height of 3.2 m and spans of 6m. In designing the building model the story drift ratios were limited to values specified by the considered code. Figure 1 presents the structural models and a typical plan of the building was considered in this study. The applied gravity loads to the structural model are presented in Table 1. Also, Tables 2 and 3 depicted the beams and columns properties of the studied building.

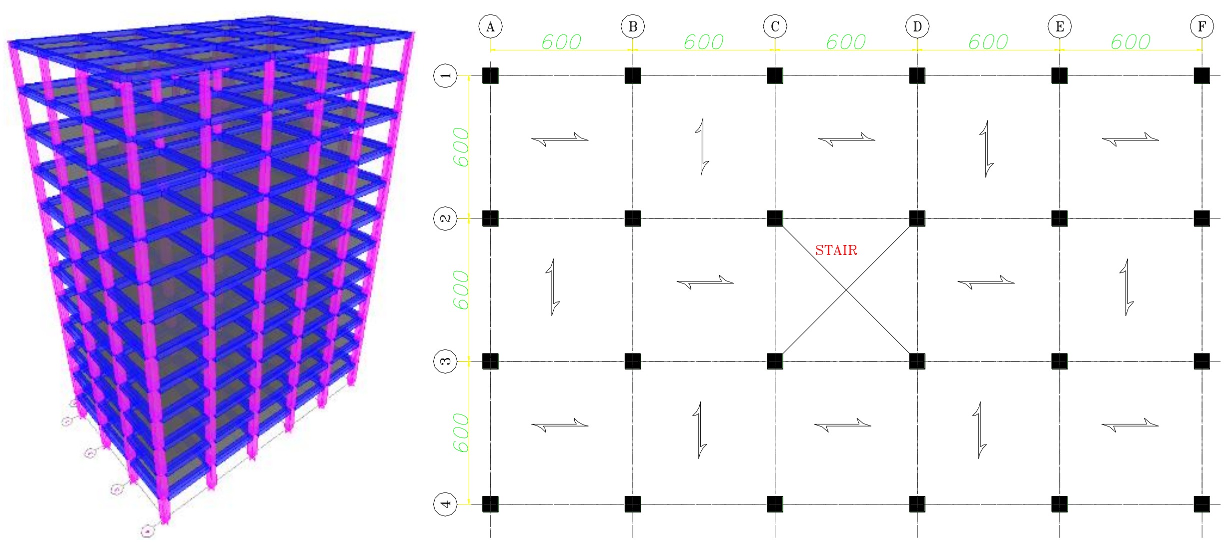

(a) (b)

Fig. 1. Structural elevation and plan: (a) 12-story building and (b) typical plan.

Table 1. Gravity loads.

Load type	*Story*	*Roof*
Dead load (Kg/m^2)	520	520
Live load (Kg/m^2)	250	150
Perimeter walls (Kg/m)	570	300

Table 2. Properties of columns in the building.

Floor	*Column Type*	*B=H (cm)*	*Cover (cm)*	*Reinforcement*
1	C1	75	5.8	28T25
2	C2	75	5.8	24T25
3	C3	75	5.8	24T25
4	C4	70	5.8	20T22
5	C4	70	5.8	20T20
6	C5	70	5.8	20T20
7	C5	65	5.8	20T20
8	C5	65	5.8	20T20
9	C6	60	5.8	20T20
10	C7	55	5.8	20T20
11	C8	50	5.8	16T20
12	C9	45	5.8	16T18

Table 3. Properties of beams in the building.

Floor	*Beam Direction*	*Beam Type*	*H (cm)*	*B(cm)*	*Top Reinforcement*	*Bot Reinforcement*
1	X	B1	65	75	8T25	7T25
	Z	G1	65	75	10T25	8T25
2	X	B2	65	75	9T25	8T25
	Z	G2	65	75	11T25	9T25
3	X	B3	65	75	9T25	8T25
	Z	G3	65	75	11T25	9T25
4	X	B4	65	70	9T25	8T25
	Z	G4	65	70	10T25	9T25
5	X	B5	65	70	9T25	7T25
	Z	G5	65	70	10T25	9T25
6	X	B6	60	70	8T25	7T25
	Z	G6	60	70	9T25	7T25
7	X	B7	60	65	10T22	8T22
	Z	G7	60	65	8T25	6T25
8	X	B8	60	65	9T22	7T22
	Z	G8	60	65	10T22	8T22
9	X	B9	55	60	8T22	6T22
	Z	G9	55	60	9T22	7T22
10	X	B10	55	55	7T22	5T22
	Z	G10	55	55	8T22	6T22
11	X	B11	55	50	5T22	4T20
	Z	G11	55	50	6T22	4T22
12	X	B12	45	45	5T20	3T20
	Z	G12	45	45	5T20	3T20

2.2. Numerical Modeling

The open system for earthquake engineering simulation (OpenSees) program [35] is applied for numerical modeling and analysis of the considered structural models. The force-based element (FBE) and displacement based element (DBE) are two techniques by OpenSees software for modeling the non-linear behavior of different structural members. In this study, "NonlinearBeamColumn" command is adopted to model the structural members using the fiber section, which is in consonance with the force formulation and considers the spread of plasticity along the element [36]. This is the most economical and accurate approach to investigate the seismic behavior of RC structures [37, 38]. The unidirectional steel and concrete layers in flexural members are illustrated in Figure 2.

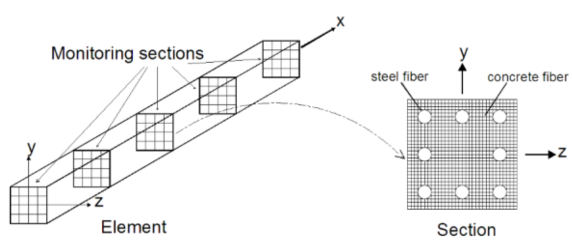

Fig. 2. Modeling flexural members using fiber command [39, 40].

The accuracy of the solution in FBE can be improved by either increasing the number of integration points or the number of elements. Rayleigh damping is used in modeling of structures. Rayleigh damping is viscous damping that is proportional to a linear combination of mass and stiffness. The damping matrix (C) is given by Equation 1, where a_0 is the mass proportional damping coefficient and a_1 is the stiffness proportional damping coefficient.

$$C=a_0.M+a_1.K \tag{1}$$

A damping ratio of 5% was assigned to the first the mode and the mode at which the cumulative mass participation exceeds 95%. The Rayleigh command allows the user to specify whether the initial, current, or last committed stiffness matrix is used in the damping matrix formulation.

It is note-worthy to mention that RC members that the core concrete, which has been confined by stirrups, has higher Compressive strength than cover concrete as a result of the so-called confinement effect. "Concrete02" material command is employed for concrete modeling in OpenSees software. In order to promote modeling accuracy, the compressive strength and strain of core concrete are determined applying the Mander-Priestly model (Figure 3) [39]. The aforementioned model is used as a general model to take confinement effects into account in different columns. Lateral reinforcements have different types such as circular, spiral and rectangular stirrup with or without ties. This project studies the structural members sections as rectangular sections with rectangular stirrup exposed to unidirectional loads. The stress-strain relationship of confined concrete has been studied widely as Equation 2:

$$f_c=\frac{f'_{cc}Xr}{r-1+X^2}\,, \qquad X=\frac{\varepsilon_c}{\varepsilon_{cc}}\,,$$

$$\varepsilon_{cc}=\left[R\left(\frac{f'_{cc}}{f_{c0}}-1\right)+1\right]\varepsilon_{c0}\,,$$

$$r=\frac{E_c}{E_c-E_{sec}} \tag{2}$$

where X represents the ratio of strain to strain at maximum stress. f'_{cc} represents the maximum stress of confined concrete. r is the ratio of the primary module of elasticity to the difference between the primary and secondary modules of elasticity. R is an empirical parameter obtained from different tests. This model suggests R=3 and R=6 for high strength concrete and typical concrete, respectively. Equation 3 gives the maximum stress of confined concrete in consonance with Mander's relation:

$$f'_{cc} = f'_{co}\left(2.254\sqrt{1+\frac{7.94f'_1}{f'_{co}}}-\frac{2f'_1}{f'_{co}}-1.254\right),$$

$$f'_1 = \frac{1}{2}K_e\rho_s f_{yh}, E_{sec} = \frac{f'_{cc}}{\varepsilon_{cc}} \quad (3)$$

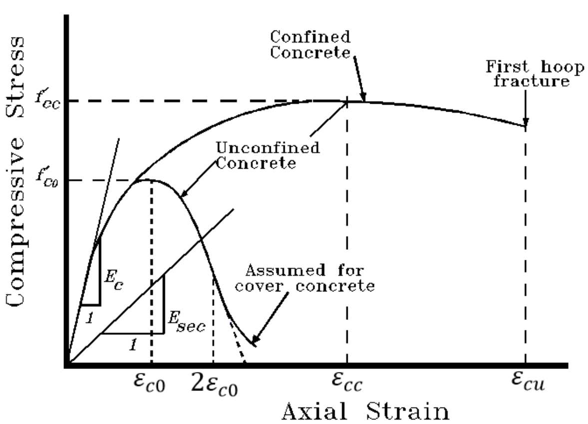

Fig. 3. Calculation of the compressive strength of confined core concrete based on Mander's model [39].

The effective confinement coefficient K_e is a very important parameter. It reveals the effectiveness of different lateral stirrups. Mander et al. [39] introduced different relations for different lateral reinforcements, especially circular and spiral stirrups, in order to calculate K_e.

$$K_e = \frac{1-kS/D"}{1-\rho_{cc}} \quad (4)$$

where ρ_{cc} represents the ratio of longitudinal reinforcement area to the core concrete section area. ρ_s is the ratio of lateral confining lateral reinforcements volume to the confined the core concrete volume. fyh is the yielding stress of lateral reinforcements. k is 0.5 for spiral and 1.0 for stirrup reinforcement. The stress-strain curves of confined core concrete in structural element sections were determined applying the KSU-RC program [40] and the Mander relationship. Rayleigh damping is used in modeling of structures. It is note-worthy to mention that, in order to avoid numerical instability or non-convergence, "Steel02" command is used for reinforcing bars modeling in OpenSees software. In the "Steel02" command, the strain-hardening ratio is considered equal to 0.01.

2.3. Soil–Structure Model

To define the coefficients of this element taking also into account soil nonlinearity, established parameters of the cone model are modified pursuant to the equivalent linear approach. To model the soil effect under the structure, the cone model (monkey-tail model) was employed with presented modifications [41]. Figure 4 demonstrates the schematic model intended for the soil-foundation element based on the cone model concept.

Table 4 presents the properties of the cones and discrete-element models representing a rigid rectangular foundation with area A_0 and area moment of inertia about the axis of rotation I_0 (for torsional rotation, I_0 is the polar moment of inertia) on the surface of homogeneous half-space. In this Table, ν is the Poisson’s ratio of the soil, Vs is the shear-wave velocity in the soil (in small strains), Vp is the P-wave velocity of the soil, ρ is density and G is the effective soil shear modulus of the soil. Initial soil shear modulus (G_0) can be obtained using geoseismic experiments and measure the shear wave velocity in small strains (Equation 4).

$$G_0 = \rho V_s^2 \quad (4)$$

Dynamic soil properties can be extremely nonlinear when ground motions are caused by large vibrations (such as design level earthquakes). As a result, the changes in the soil shear modulus and material damping ratio with shearing strain amplitude must be accounted for in the ground response analysis. The linear solution, which is applicable for small vibration levels, can be modified to overcome this problem. One approach to handling nonlinear soil behavior due to the shaking during a design level event is to perform linear analyses with dynamic soil properties that are iterated in a manner consistent with an "effective" shearing strain induced in the soil layer [42, 43]. This iterative approach is called "equivalent linear analysis". The effective soil shear modulus, G, which decreases with increasing strain, can be estimated in terms of the initial soil shear modulus (G_0), cite class and peak ground acceleration according to Equation 5.

$$G = G_0 \times \left(\frac{G}{G_0}\right) \tag{5}$$

where $\left(\frac{G}{G_0}\right)$ is the effective shear modulus ratio that shall be calculated in accordance with ASCE/SEI 41-06 [44]. It should be noted that, Stiffness coefficients of foundation in table 4 were calculated for rectangle shaped foundations (L×B, L>B).

Table 4. con model of properties of the rectanqular foundation on a homogeneous half-space [41].

Motion	Horizontal	Vertical		Rocking		Torsion
equivalent radius (r_0)	$\sqrt{\frac{A_0}{\pi}}$	$\sqrt{\frac{A_0}{\pi}}$		$\sqrt[4]{\frac{4I_0}{\pi}}$		$\sqrt[4]{\frac{2I_0}{\pi}}$
Aspect ratio $\frac{z_0}{r_0}$	$\frac{\pi}{8}(2-\upsilon)$	$\frac{\pi}{4}(1-\upsilon)(\frac{V}{V_s})^2$		$\frac{9\pi}{32}(1-\upsilon)(\frac{V}{V_s})^2$		$\frac{9\pi}{32}$
Poisson's ratio	All value	$\nu \le 1/3$	$1/3<\nu\le 1/2$	$\nu \le 1/3$	$1/3<\nu\le 1/2$	All value
wave velocity (V)	V_s	V_p	$2V_s$	V_p	$2V_s$	V_s
added mass	0	0	$2.4(\upsilon-\frac{1}{3})\rho A_0 r_0$	0	$1.2(\upsilon-\frac{1}{3})\rho A I_0 r_0$	0
Lumped-parameter model	$K_x = \frac{GB}{2-\upsilon}\left[3.4\left(L/_B\right)^{0.65}+1.2\right]$ $K_y = \frac{GB}{2-\upsilon}\left[3.4\left(L/_B\right)^{0.65}+0.4\,L/_B+0.8\right]$ $K_z = \frac{GB}{1-\upsilon}\left[1.55\left(L/_B\right)^{0.75}+0.8\right]$ $C = \rho.V.A_0$ $C' = \frac{2\xi_0}{\omega_0}K,\ m' = \frac{\xi_0}{\omega_0}C$			$K_{xx} = \frac{GB^3}{1-\upsilon}\left[0.4\left(L/_B\right)+0.1\right]$ $K_{yy} = \frac{GB^3}{1-\upsilon}\left[0.4\left(L/_B\right)^{2.4}+0.034\right]$ $K_{zz} = GB^3\left[0.53\left(L/_B\right)^{2.45}+0.51\right]$ $C_\theta = \rho.V.I_0,\ C_\theta{}' = \frac{2\xi_0}{\omega_0}K_\theta$ $M_\theta = \rho I_0 z_0,\ m_\theta{}' = \frac{\xi_0}{\omega_0}C_\theta$		

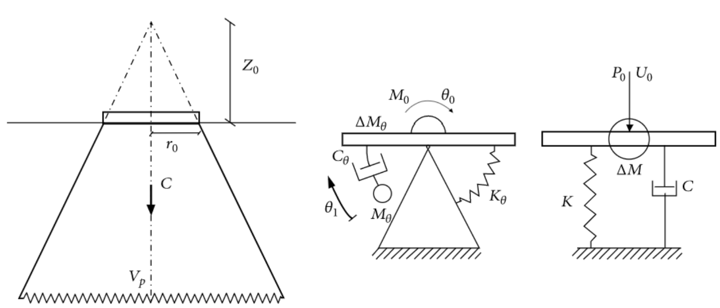

Fig. 4. Cone Model layout and equivalent lumped elements for soil replacement model [41].

To model sub-structure employing the monkey-tail model, two nodes at the same location have been defined at the base level. Applying spring stiffness independent of frequency and a damping coefficient into account the frequency dependence of the interaction is the easiest way to deliberate the effects of SSI. The nodes have been connected by multiple Uniaxial Material objects base on the cone model. All degree of freedom in the first node and Vertical degree of freedom in the second node have been constrained. The springs and dampers have been connected from the first node to the second node using a zero-length element and the vertical degree of freedom was ignored. In addition, the masses of the separated model have been applied to the second node. The soil Poisson's coefficient, soil damping ratio, and soil density, as the essential parameters for soil modeling, were contemplated to be 0.33, 0.05 and 2000 kg/m^3.

2.4. Validation of the Mathematical Model

In order to evaluate the validity of the employed model, the bridge column subjected to the loading protocol which is illustrated in Figure 5 [36] is considered. (Lehman & Moehle, PEER 1998/01 (Column 415)). The column model is calibrated using the force-based element with 5 integration points. In order to gain the best compatibility between the numerical modeling and experimental results, five integration points were selected. In this case, the column had to be modeled with one force based element (FBE). Local response quantities could not be compared due to the lack of experimental data. The results are demonstrated in Figure 6. In addition, to evaluate the validity of the structural model in OpenSees, the variation of the fundamental periods of the 12-story building model is compared with the result of ETABS software. Table 5 presents that the fundamental period of the 12- story structure are close together with acceptable accuracy in two cases.

Table 5. The fundamental period of 12 story structure for different software.

Period (sec)	T_1	T_2
ETABS	1.3749	1.2939
OpenSees	1.3753	1.3089

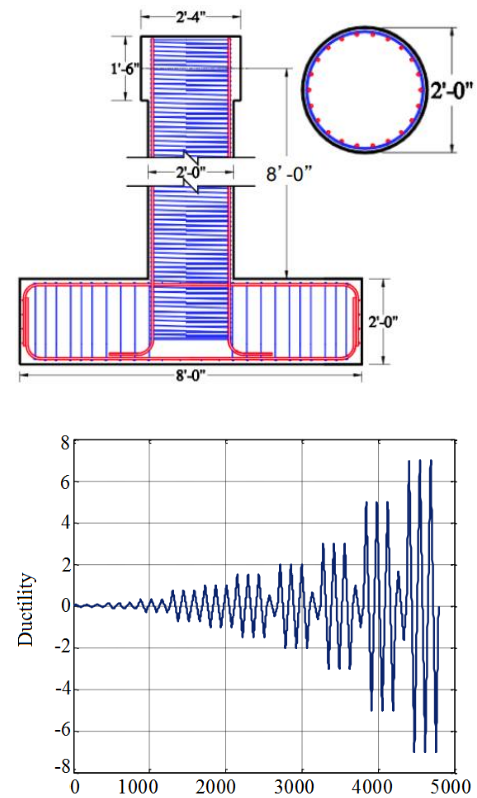

Fig. 5. Bridge column detail and cyclic loading protocol [36].

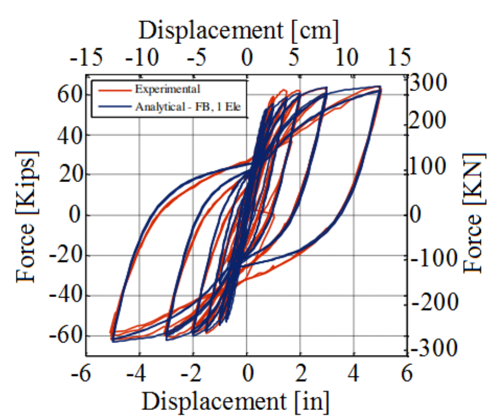

Fig. 6. Comparing the results of numerical modeling with FBE and experimental results [36].

2.5. The Earthquake Records Used for Parametric Studies

23 pairs of far-field earthquake records have been selected from PEER [45] that have mostly been applied in FEMA-440 [46]. Table 6 reveals the specification of the selected earthquake records that have been registered on stiff soil (soil type D with shear wave velocity of 180m/s to 360m/s) resulting from events with a magnitude of 6.2 to 7.3 and fault distance of 21.2 to 50.7km. The selected records were normalized confirming to the ASCE 7-10 code [33] before being used in the extensive nonlinear dynamic time history analyses.

Table 6. Specification of earthquake records for the numerical analyses.

No	Date	Earthquake Name	Record name	Magnitude (Ms)	Station number	PGA(g)	Vs(m/s)
1	01/17/94	Northridge	NORTHR /MUL279	6.7	90013	0.516	356
			NORTHR /MUL009			0.416	
2	01/17/94	Northridge	NORTHR /LOS270	6.7	90057	0.482	309
			NORTHR /LOS0			0.41	
3	01/17/94	Northridge	NORTHR /HOL90	6.7	24303	0.358	256
			NORTHR /HOL360			0.231	
4	11/12/1999	Duzce,Turkey	Duzce /BOL090	7.3	Bolu	0.822	326
			Duzce/BOL0			0.728	
5	10/15/79	Impeial Valley	IMPVALL\H-DLT352	6.9	6605	0.351	275
			IMPVALL\H-DLT262			0.238	
6	10/15/79	Impeial Valley	IMPVALL\H-EL1230	6.9	5058	0.38	196
			IMPVALL\H-EL140			0.364	
7	10/15/79	Impeial Valley	IMPVALL\H-CHI012	6.9	6621	0.27	256
			IMPVALL\H-CHI282			0.254	
8	11/24/87	Superstitn Hills(B)	SUPERST/ B-CAL315	6.6	5061	0.247	208
			SUPERST/ B-CAL225			0.18	
9	8/17/99	Kocaeli,Turkey	KOCAELI\ DZC270	7.8	Duzce	0.358	276
			KOCAELI \DZC180			0.312	
10	10/01/1987	Whittier Narrows	WHITTIER /A-BIR180	5.7	90079	0.299	276
			WHITTIER /A-BIR090			0.243	
11	06/28/92	Landers	LANDERS /YER270	7.4	22074	0.245	354
			LANDERS /YER360			0.152	
12	06/28/92	Landers	LANDERS /CLW-TR	7.4	23	0.417	271
			LANDERS /CLW-LN		Coolwater	0.283	
13	10/18/89	Loma Preita	LOMAP /CAP000	7.1	47125	0.529	289
			LOMAP /CAP090			0.443	
14	10/18/89	Loma Preita	LOMAP /GO3000	7.1	47381	0.555	350
			LOMAP /GO3090			0.367	
15	10/18/89	Loma Preita	LOMAP /SLC360	7.1	1601	0.278	289
			LOMAP /SLC270			0.194	
16	11/24/87	Superstitn Hills(B)	SUPERST /B-ICC000	6.6	1335	0.358	192
			SUPERST /B-BICC090			0.258	

No	Date	Earthquake Name	Record name	Magnitude (Ms)	Station number	PGA(g)	Vs(m/s)
17	11/24/87	Superstitn Hills(B)	SUPERST /B-POE270	6.6	Poe Road	0.446	208
			SUPERST /B-POE360			0.3	
18	04/25/92	Cape Mendocino	CAPEMEND/RIO360	7.1	89324	0.549	312
			CAPEMEND/RIO270			0.385	
19	09/20/99	Chi-Chi Taiwan	CHICHI/CHY101-N	7.6	CHY101	0.44	259
			CHICHI/ CHY101-W			0.353	
20	04/24/84	Morgan Hill	MORGAN/HD4165	6.1	1656	0.098	256
			MORGAN/HD4255			0.092	
21	02/09/1971	San Fernando	SFERN/PEL090	6.6	135 LA	0.21	316
			SFERN /PEL180			0.174	
22	05/02/1983	Coalinga	COALINGA/H-C05270	6.5	36227	0.147	256
			COALINGA/H-C05360			0.131	
23	01/16/95	Kobe	KOBE/ SHI000	6.9	Shin-Osaka	0.243	256
			KOBE/ SHI090			0.212	

3. Analysis and Results

Following the selection and normalization of the earthquake records and preparation of the structural models, the IDA analyses were conducted applying the OpenSees program [35] under the applied bi-directional seismic excitations. In the process of modeling, both types of the one- and two-way mass center eccentricities in the range of $0-20\%$ of the building's plan dimensions are taken into account by proper shifting the mass centers of all stories. Also, the SSI effect was inquired corresponded to the median and dispersion of collapse fragility curves. The IDA curves were developed considering the $S_a(T1, \zeta=5\%)$ as scalar intensity measures (IM). It is worth noting that the selection of an intensity measure (IM) depends on the efficiency in terms of seismic intensity and on the sufficiency in terms of the number of earthquake records. Generally, the purpose of this feature is to reduce the dependence of the results on records specifications. If there is no near field earthquake caused directivity effects in seismic records, selecting $S_a(T1,5\%)$ for moderate height will be sufficient for describing the primary specifications of ground motion in structural responses [47]. In this way, sufficient accuracy in the estimation of seismic demand and capacity can be obtained using fewer records (10 to 20 ground motion records) with no dependency of results on record intensity. The dispersion of IDA curves for different engineering demand parameters (EDP) was determined in different mass center eccentricities of the building. The maximum square root of the sum of the squares of IDRx and IDRz were selected as EDP in IDA curves (IDRsrss). Figures 7 and 8 present the IDA curves generated for the 12-story building under different one-way mass center eccentricities in two states of fixed-base and considering SSI. Moreover, the IDA curves corresponding to the different two-way eccentricities with fixed- and flexible- base are portrayed in figures 9 and 10.

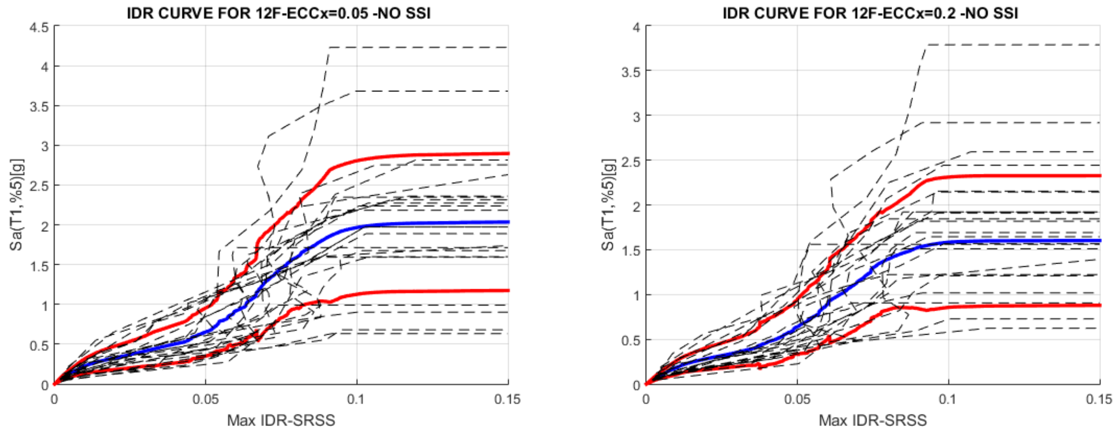

(a) (b)

Fig. 7. IDA curves of the 12-story building with the fixed-base assumption (a) with a one-way eccentricity of 5% (b) with a one-way eccentricity of 20%.

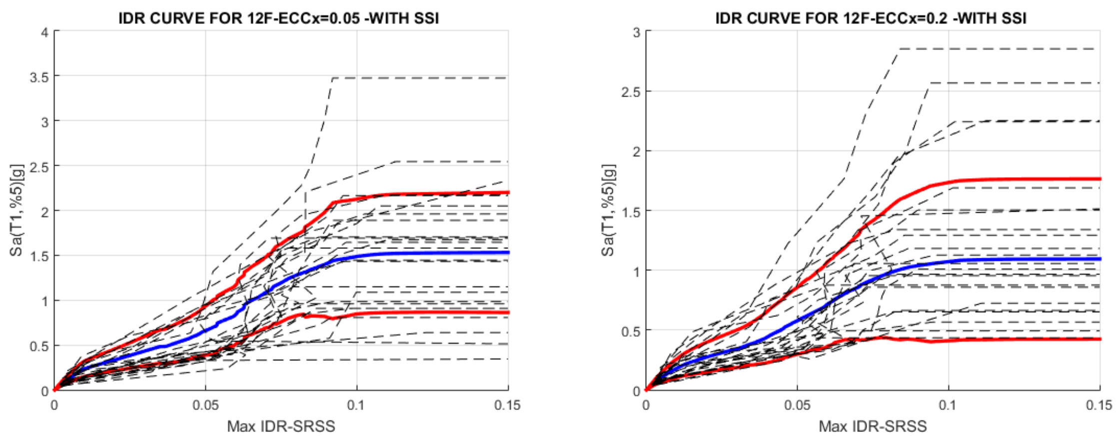

(a) (b)

Fig. 8. IDA curves of the 12-story building with considering SSI (a) with a one-way eccentricity of 5% (b) with a one-way eccentricity of 20%.

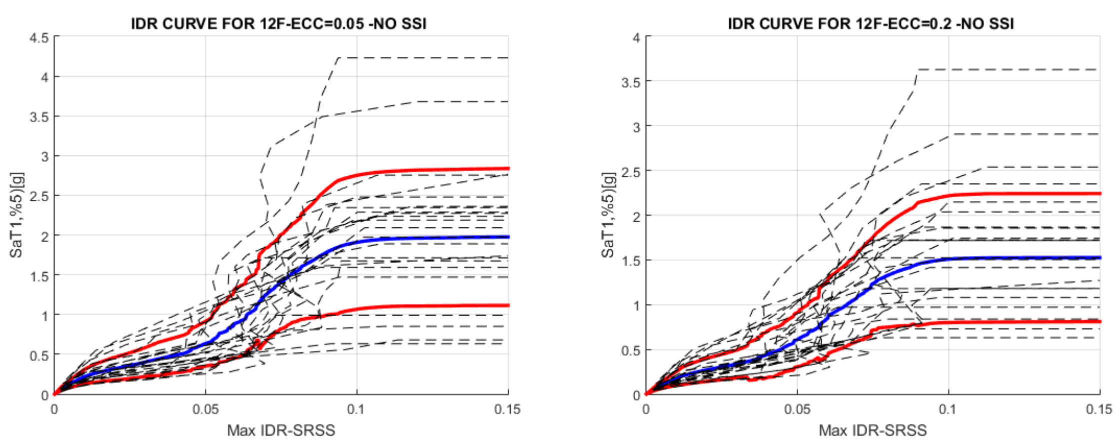

(a) (b)

Fig. 9. IDA curves of the 12-story building with the fixed-base assumption (a) with a two-way eccentricity of 5% (b) with a two-way eccentricity of 20%.

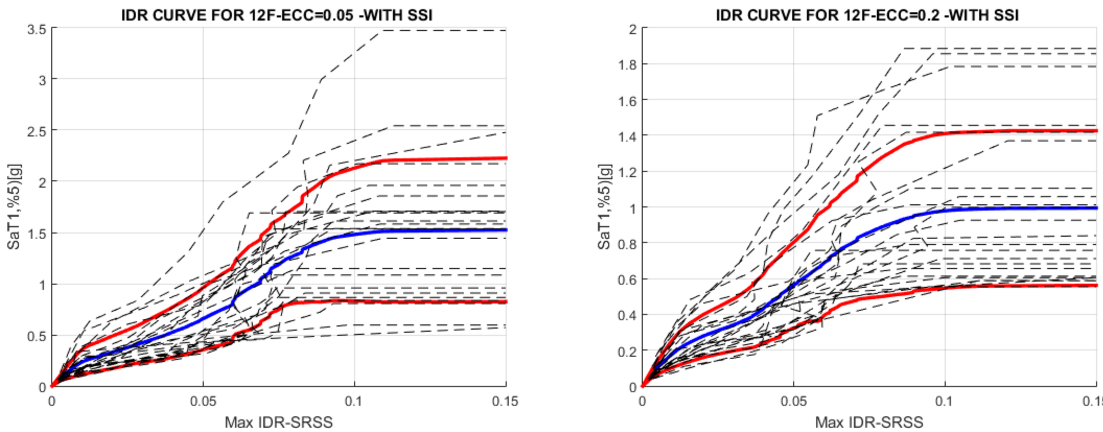

(a) (b)

Fig. 10. IDA curves of the 12-story building with considering SSI (a) with a two-way eccentricity of 5% (b) with a two-way eccentricity of 20%.

3.1. Estimation of Collapse Fragility Curves with Fixed-Base Assumption

To extract the occurrence probability of collapse from IDA results, the so-called fragility curves are employed. Collapse fragility curve can be considered as a log-normal cumulative distribution function (CDF) of a stochastic variable namely collapse capacity (S_{ac}). Ibarra and krawinkler demonstrated that S_{ac} points follow a log-normal distribution i.e. $\mathrm{Ln}(S_{ac}) \rightarrow N(\eta_C, \beta_{RC})$ where η_C and β_{RC} are median and dispersion of the collapse capacity values due to different earthquake records which are numerically equal to the standard deviation of collapse capacity values [48]. For a given hazard level, like PR, corresponding spectral acceleration can be obtained using seismic hazard curves and collapse probability can be calculated from Equation 6, where η_C and β_{RC} are median and standard deviation of the log-normal cumulative distribution function, respectively:

$$P(C|S_a^{PR}) = \Phi(\frac{Ln(S_a^{PR}) - Ln(\eta_C)}{\beta_{RC}}) \qquad (6)$$

In this study, two methods for estimation of the median and dispersion values of fragility curves of the studied building are discussed. In the first approach, collapse fragility curves estimated directly in consonance with the calculation of the median and the dispersion of logarithmic data points (Direct Method) and in the second approach, the collapse fragility curves estimate using the fitting the log-normal distribution to collapse capacity data points (Fitting Method). Figures 11 and 12 present the collapse fragility curves of the 12-story building with fixed-base assumption under one- and two-way different mass center eccentricities based on two mentioned approaches. Furthermore, the simultaneous effects of the horizontal components of the selected earthquake records were considered to estimate the fragility curves. Collapse capacity values (S_{ac}) obtained from the IM-based approach for the estimation of the collapse fragility curve [49].

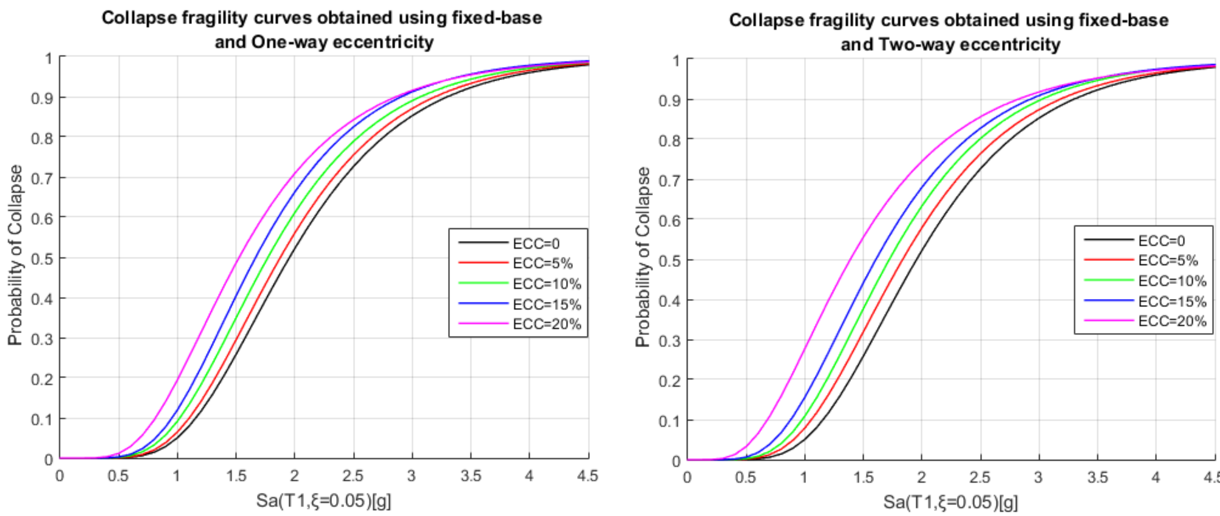

(a) (b)

Fig. 11. Collapse fragility curves obtained using the direct method and fixed-base assumption: (a) One-way mass centers eccentricities, (b) two-way mass centers eccentricities.

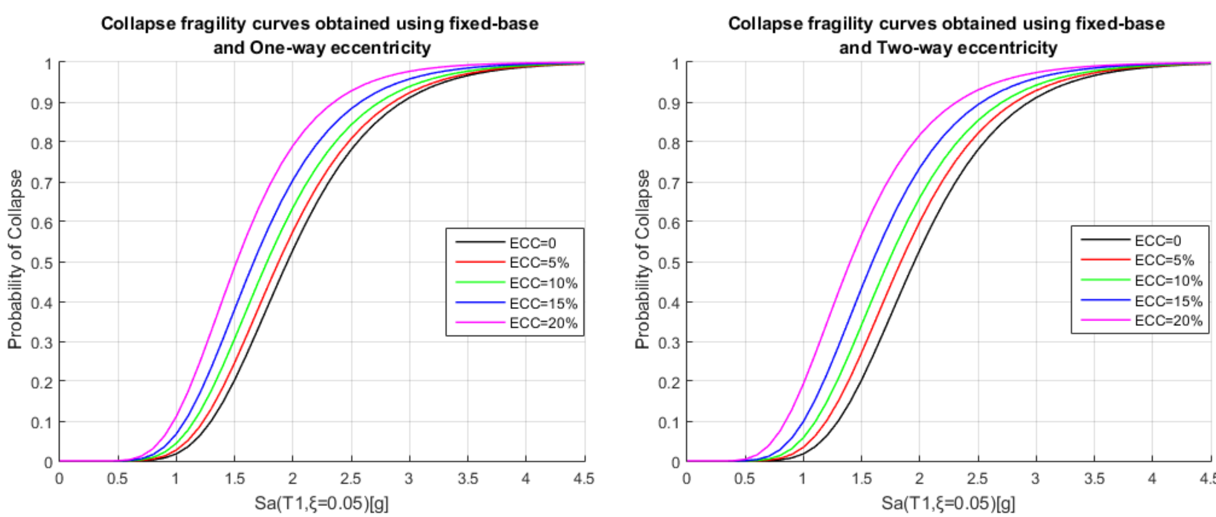

(a) (b)

Fig. 12. Collapse fragility curves obtained using the fitting method and fixed-base assumption: (a) One-way mass centers eccentricities, (b) two-way mass centers eccentricities.

Table 7 presents the median (η_C) and standard deviation (β_{RC}) of the fragility curve of the studied building with fixed-based in the form of the log-normal cumulative distribution function. It is note-worthy to mention that, collapse fragility curves obtained by the fitting method give the lower dispersion value. Moreover, the median of the collapse capacities (by fixed-base assumption) decreases respectively by $3.84\% - 22.36\%$ and $5.93\% - 28.22\%$ for one- and two-way eccentricities in the range of the 5% to 20% of the building's plan dimensions.

Table 7. The fragility curve parameters obtained by fixed-base assumption using various methods.

Estimation method	Eccentricities type	Statistical Parameters	Percentage of the mass center eccentricities				
			Ecc=0	Ecc=5%	Ecc=10%	Ecc=15%	Ecc=20%
Direct method	One-way	median(μ)	1.9543	1.8762	1.7703	1.6656	1.5250
		Standard deviation(β_{RC})	0.4089	0.4156	0.4298	0.4346	0.4913
	Two-way	median(μ)	1.9543	1.8350	1.7213	1.6065	1.3880
		Standard deviation(β_{RC})	0.4089	0.4299	0.4402	0.4684	0.5544
Fitting Method	One-way	median(μ)	1.9531	1.8780	1.7786	1.6641	1.5163
		Standard deviation(β_{RC})	0.3183	0.3280	0.3377	0.3412	0.3419
	Two-way	median(μ)	1.9531	1.8371	1.7300	1.5925	1.4020
		Standard deviation(β_{RC})	0.3183	0.3341	0.3497	0.3617	0.3913

3.2. Estimation of Collapse Fragility Curves with SSI Consideration

In this section, collapse fragility curves of the studied building were obtained employing the SSI consideration for soil type D. As in the previous section, mass centers of all stories were shifted in the range of the $0\% - 20\%$ of the building's plan dimensions and in the form of one- and two-way mass center eccentricities. In addition, the fragility curves were obtained applying two mentioned approaches. Figures 13 and 14 present the collapse fragility curves of the studied building based on the two types of the mentioned methods under the various eccentricities. Since the fragility curves are in the form of the log-normal cumulative distribution function with median (η_C) and standard deviation (β_{RC}) parameters, their values are summarized in Table 8.

Inspecting figures 13 and 14 reveals that fitting method estimated the lower values for the dispersion and median of the collapse fragility curve compared with the direct method, so it can be concluded that fitting method can lead to more comprehensive and sufficient results. Table 8 presents that increasing the one-way eccentricity of the mass centers in all stories from 5% to 20% of the building's dimensions in flexible-base (SSI effect) decreases the median of the collapse fragility curve by 5.44%-29.49%. Moreover, by considering the two-way eccentricities in the range of the 5% to 20% of the building's dimensions, the median of the collapse fragility curve has been decreased by 9.74%-38%, respectively. By proper shifting the mass centers from 0 to 20% of the building's dimensions in all stories, fixed-base assumption overestimates the median of the collapse capacities in the range of 29.87%-39.45% compared with the

SSI consideration. The results of this comparison are reported in Figure 15. The results reveal that in the absence of the mass center eccentricities, the fixed-base assumption overestimates the median of collapse capacity as much as 29.87% compared with the SSI consideration. Moreover, in one- and two-way eccentricity of mass centers equal to 20% of the building dimensions, fixed-base assumption in comparison with the SSI consideration for soil type D overestimates the median of the collapse capacity by 36.3% and 39.45%. This difference is significant and cannot be neglected, respectively. In addition, the presence of torsion and consideration of the SSI effect increase the dispersion of the fragility curve.

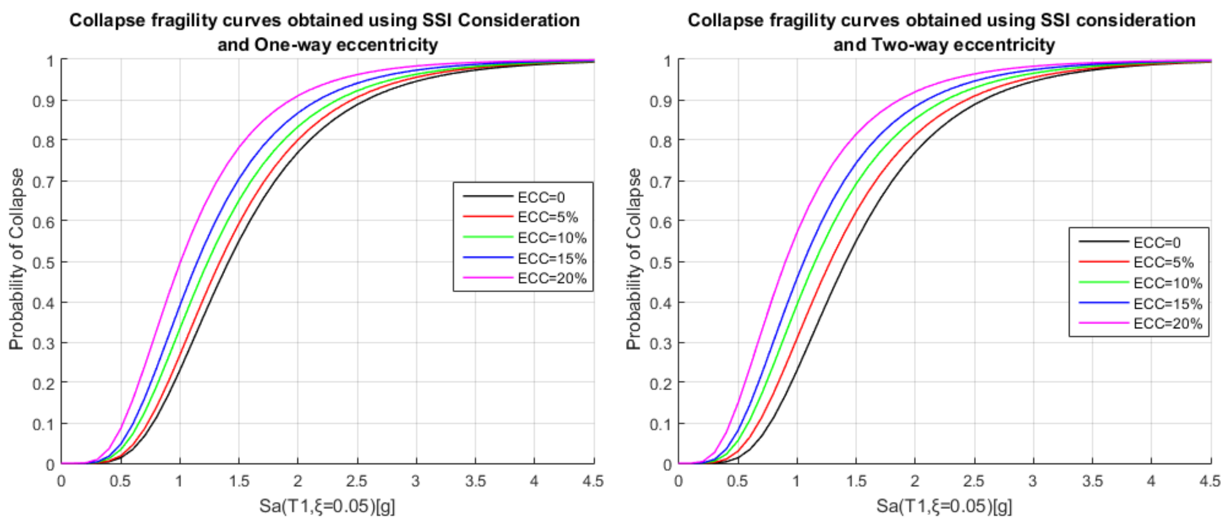

(a) (b)

Fig. 13. Collapse fragility curves obtained using the direct method with SSI consideration: (a) One-way mass centers eccentricities, (b) two-way mass centers eccentricities.

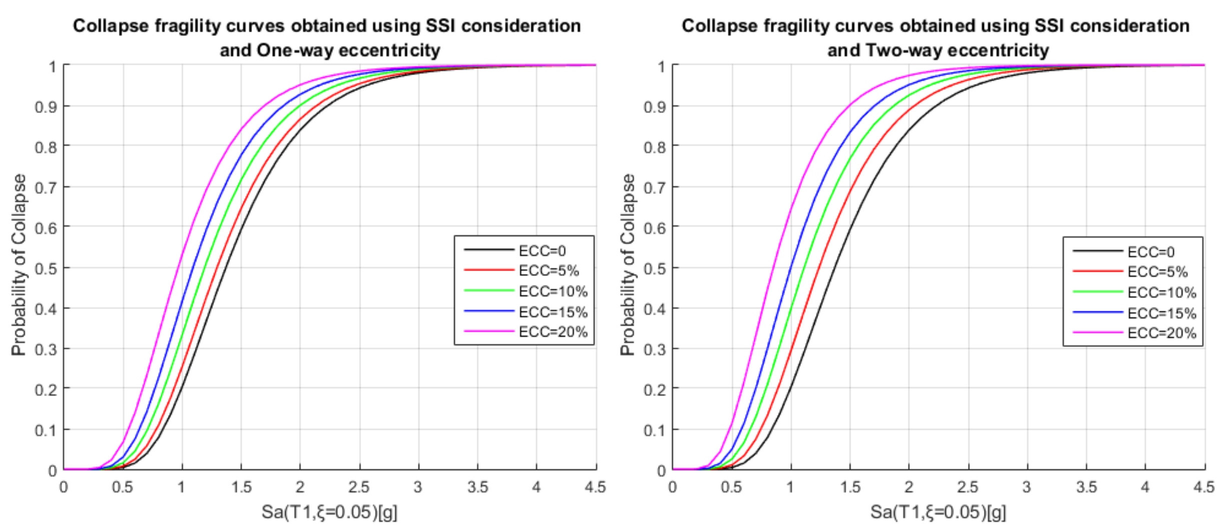

(a) (b)

Fig. 14. Collapse fragility curves obtained using the fitting method with SSI consideration: (a) One-way mass centers eccentricities, (b) two-way mass centers eccentricities.

Table 8. The fragility curve parameters obtained by SSI consideration using various methods.

Estimation method	Eccentricities type	Statistical Parameters	Percentage of the mass center eccentricities				
			Ecc=0	Ecc=5%	Ecc=10%	Ecc=15%	Ecc=20%
Direct Method	One-way	median(μ)	1.4125	1.3390	1.2369	1.1473	1.0053
		Standard deviation(β_{RC})	0.4694	0.4737	0.4955	0.4980	0.5126
	Two-way	median(μ)	1.4125	1.2812	1.1519	1.0561	0.9013
		Standard deviation(β_{RC})	0.4694	0.5006	0.5260	0.5355	0.5677
Fitting Method	One-way	median(μ)	1.3696	1.2950	1.1901	1.0916	0.9656
		Standard deviation(β_{RC})	0.3808	0.3912	0.4037	0.4151	0.4400
	Two-way	median(μ	1.3696	1.2361	1.1104	1.0023	0.8489
		Standard deviation(β_{RC})	0.3808	0.3929	0.4077	0.4197	0.4404

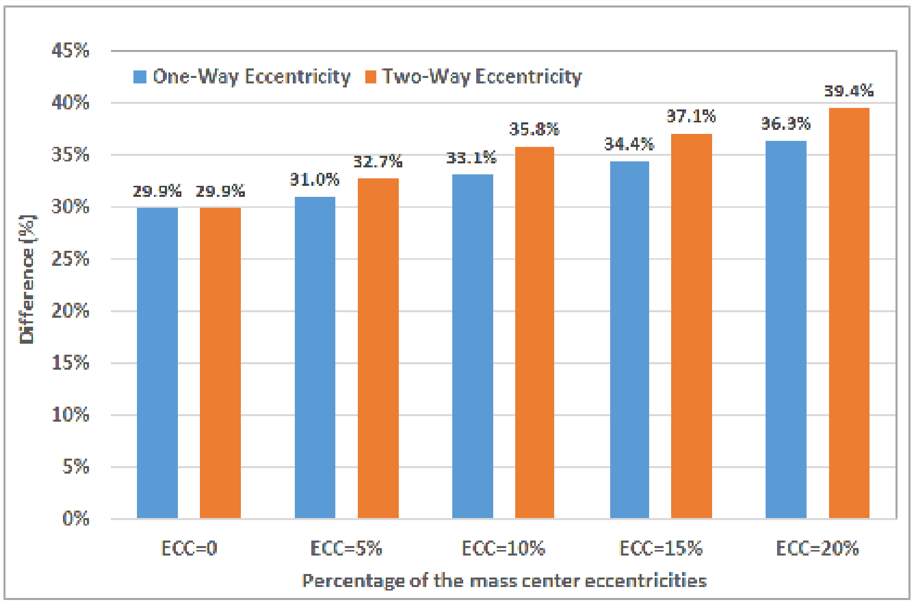

Fig. 15. Differences between the median of the fragility curves due to fixed-based assumption and SSI.

4. Conclusions

In this paper, a 12-story RC moment resisting building considering both types of the one- and two-way eccentricities and regular elevation subjected to bi-directional ground motions is presented. By deliberating the non-linear behaviors of reinforcing bars as well as cover and confined concrete materials, the effect of torsion, both types of the fixed-base assumption and contemplating of the soil-structure interaction (SSI) is employed in order to estimate the parameters of the collapse fragility curve. Incremental dynamic analysis (IDA) was conducted to take the uncertainties of earthquake records into account. Also, the accuracy of the two methods in the estimation of the collapse fragility curve was discussed. It could be concluded that estimation of the parameters of the collapse fragility curves by fitting the log-normal distributions to the collapse capacity points reduces the uncertainty of record to record in seismic behavior study and increases the reliability of results.

In the studied building, increasing the torsion can be decreased the median of the collapse capacities. Moreover, increasing the torsion can be increased the dispersion of the fragility curve in direct and fitting methods. It is note-worthy to mention that, fixed-base assumption overestimates the median of collapse capacity by $29.87\% - 39.45\%$ in the presence of torsion due to one- and two-way eccentricities, respectively. Moreover, if there is no torsion in the building, assuming fixed-base overestimates the median of collapse fragility curve by 29.87% compared with SSI consideration. In addition, the fixed-based condition illustrates an underestimation of the dispersion value of the collapse fragility curves in range by 0.049-0.098 in comparison with the SSI conditions. Finally, the fixed-base assumption with the existence of the mass centers eccentricity of all stories as much as 20% of the building's dimensions can be overestimated respectively the median of the collapse capacity of building in one- and two-way eccentricities by 36.3% and 39.45%.

It should be pointed out that, presences of the torsion in the studied building with fixed-based assumption can significantly escalate the discrepancies of the median of the collapse capacity. This fact is more essential. Therefore, eventually, it can be stated that considering of the SSI effect for building with one- or two-way mass center eccentricities up to 20% of the building's plan dimensions is a curial case for fragility curve analysis.

REFERENCES

[1] Jalayer, F., & Cornell, C. A. (2003). “A technical framework for probability-based demand and capacity factor (DCFD) seismic formats.” RMS.

[2] Cornell, C. A., Jalayer, F., Hamburger, R. O., Foutch, D. A. (2002). “Probabilistic basis for 2000 SAC federal emergency management agency steel moment frame guidelines.” Journal of structural engineering, Vol. 128 no.4, pp. 526-533.

[3] Ibarra, L. F., Krawinkler, H. (2005). “Global collapse of frame structures under seismic excitations.” Berkeley, CA: Pacific Earthquake Engineering Research Center, pp. 29-51.

[4] Haselton, C. B., Liel, A. B., Dean, B. S., Chou, J. H., Deierlein, G. G. (2007). “Seismic collapse safety and behavior of modern reinforced concrete moment frame buildings.” In Structural engineering research frontiers, pp. 1-14.

[5] Zareian, F., Krawinkler, H. (2007). “Assessment of probability of collapse and design for collapse safety.” Earthquake Engineering & Structural Dynamics, Vol. 36(13), pp. 1901-1914.

[6] Vamvatsikos, D., Cornell, C. A. (2002). “Incremental dynamic analysis.” Earthquake Engineering & Structural Dynamics, Vol. 31(3), pp. 491-514.

[7] Stoica, M., Medina, R. A., McCuen, R. H. (2007). “Improved probabilistic quantification of drift demands for seismic evaluation.” Structural Safety, Vol. 29(2), pp. 132-145.

[8] Kappos, A. J., Panagopoulos, G. (2010). “Fragility curves for reinforced concrete buildings in Greece.” Structure and Infrastructure Engineering, Vol. 6(1-2), pp. 39-53.

http://dx.doi.org/10.1080/15732470802663771

[9] Haselton, C. B., Liel, A. B., Deierlein, G. G., Dean, B. S., Chou, J. H. (2010). “Seismic

collapse safety of reinforced concrete buildings. I: Assessment of ductile moment frames." Journal of Structural Engineering, Vol. 137(4), pp. 481-491.

[10] Lignos, D. G., Hikino, T., Matsuoka, Y., Nakashima, M. (2012). "Collapse assessment of steel moment frames based on E-Defense full-scale shake table collapse tests." Journal of Structural Engineering, Vol. 139(1), pp. 120-132.

[11] Palermo, M., Hernandez, R. R., Mazzoni, S., Trombetti, T. (2014). "On the seismic behavior of a reinforced concrete building with masonry infills collapsed during the 2009 L'Aquila earthquake." Earthquake and Structures, Vol. 6(1), pp. 45-69.

[12] Bolisetti, C. (2014). "Site response, soil-structure interaction and structure-soil-structure interaction for performance assessment of buildings and nuclear structures." (Doctoral dissertation, State University of New York at Buffalo).

[13] ATC-3-06 (1978). "Amended tentative provisions for the development of seismic regulations for buildings." ATC publications ATC 3-06, NBS Special Publication 510, NSF Publication 78-8, Applied Technology Council. US Government Printing Office: Washington DC.

[14] NEHRP Consultants Joint Venture. (2012). Soil-Structure Interaction for Building Structures. NIST GCR. http://doi.org/12-917-21

[15] NIST GCR 12-917-21 (2012). "Soil-Structure Interaction for Building Structures". U.S. Department of Commerce National Institute of Standards and Technology Engineering Laboratory Gaithersburg, MD 20899, September 2012.

[16] Renzi, S., Madiai, C., Vannucchi, G. (2013). "A simplified empirical method for assessing seismic soil-structure interaction effects on ordinary shear-type buildings." Soil Dynamics and Earthquake Engineering, Vol. 55, pp. 100-107.

[17] Saouma, V., Miura, F., Lebon, G., Yagome, Y. (2011). "A simplified 3D model for soil-structure interaction with radiation damping and free field input." Bulletin of Earthquake Engineering, Vol. 9(5), pp. 1387.

[18] Rayhani, M. T., El Naggar, M. H. (2012). "Physical and numerical modeling of seismic soil-structure interaction in layered soils." Geotechnical and Geological Engineering, Vol. 30(2), pp. 331-342.

[19] Pecker, A., Paolucci, R., Chatzigogos, C., Correia, A. A., & Figini, R. (2014). "The role of non-linear dynamic soil-foundation interaction on the seismic response of structures." Bulletin of Earthquake Engineering, Vol. 12(3), pp. 1157-1176.

[20] Sáez, E., Lopez-Caballero, F., Modaressi-Farahmand-Razavi, A. (2013). "Inelastic dynamic soil–structure interaction effects on moment-resisting frame buildings." Engineering structures, Vol. 51, pp. 166-177.

[21] Figini, R., Paolucci, R. (2017). "Integrated foundation–structure seismic assessment through non-linear dynamic analyses." Earthquake Engineering & Structural Dynamics, Vol. 46(3), pp. 349-367.

[22] Raychowdhury, P. (2011). "Seismic response of low-rise steel moment-resisting frame (SMRF) buildings incorporating nonlinear soil–structure interaction (SSI)." Engineering Structures, 33(3), 958-967.

[23] Khoshnoudian, F., Ahmadi, E., Kiani, M., Tehrani, M. H. (2015). "Dynamic instability of Soil-SDOF structure systems under far-fault earthquakes." Earthquake Spectra, Vol. 31(4), pp. 2419-2441.

[24] Ghandil, M., & Behnamfar, F. (2015). "The near-field method for dynamic analysis of structures on soft soils including inelastic soil–structure interaction." Soil Dynamics and Earthquake Engineering, Vol. 75, pp. 1-17.

[25] Ghandil, M., Behnamfar, F., Vafaeian, M. (2016). “Dynamic responses of structure–soil–structure systems with an extension of the equivalent linear soil modeling.” Soil Dynamics and Earthquake Engineering, Vol. 80, pp. 149-162.

[26] Anvarsamarin, A., Rofooei, F. R., Nekooei, M. (2018). “Soil-Structure Interaction Effect on Fragility Curve of 3D Models of Concrete Moment-Resisting Buildings.” Shock and Vibration, Vol. 2018.

[27] Shakib, H., Homaei, F. (2017). “Probabilistic seismic performance assessment of the soil-structure interaction effect on seismic response of mid-rise setback steel buildings.” Bulletin of Earthquake Engineering, Vol. 15(7), pp. 2827-2851.

[28] Behnamfar, F., Banizadeh, M. (2016). “Effects of soil–structure interaction on distribution of seismic vulnerability in RC structures.” Soil Dynamics and Earthquake Engineering, Vol. 80, pp. 73-86.

[29] Ghandil M., Behnamfar F. (2017). “Ductility demands of MRF structures on soft soils considering soil-structure interaction”, Soil Dynamics and Earthquake Engineering Vol. 92, pp. 203–214.

[30] Karapetrou, S. T., Fotopoulou, S. D., Pitilakis, K. D. (2015). “Seismic vulnerability assessment of high-rise non-ductile RC buildings considering soil–structure interaction effects.” Soil Dynamics and Earthquake Engineering, Vol. 73, pp. 42-57.

[31] Pitilakis, K., Crowley, H., Kaynia, A. M. (2014). “SYNER-G: typology definition and fragility functions for physical elements at seismic risk.” Geotechnical, Geological and Earthquake Engineering, Vol, 27.

[32] ACI Committee, American Concrete Institute, International Organization for Standardization. (2008). “Building code requirements for structural concrete (ACI 318-08) and commentary”. American Concrete Institute.

[33] ASCE 7-10. (2010). “Minimum Design Loads for Buildings and Other Structures.” American Society of Civil Engineers, Reston, VA, USA.

[34] ETABS, Structural Analysis Program, Computers and Structures Inc. (2013). Berkeley, CA, USA.

[35] OpenSees (2011). “Open System for Earthquake Engineering Simulation.” University of Berkeley, Berkeley, CA, USA.

http://opensees.berkeley.edu/wiki/index.php/Main_Page.

[36] Terzic, V. (2011). “Force-based element vs. Displacement-based element.” University of Berkeley, OpenSees, NEES, & NEEScomm.

[37] Spacone, E., Filippou, F. C., Taucer, F. F. (1996). “Fibre beam–column model for non-linear analysis of R/C frames: Part I. Formulation.” Earthquake Engineering & Structural Dynamics, Vol. 25, no. 7, pp. 711-725.

[38] Spacone, E., Filippou, F. C., Taucer, F. F. (1996). “Fibre beam–column model for non-linear analysis of R/C frames: part II. Applications.” Earthquake engineering and structural dynamics, Vol. 25, no. 7, pp. 727-742.

[39] Mander J B., Priestley M J N., Park R. (1988). “Observed stressstrain behavior of confined concrete.” Journal of Structural Engineering, Vol. 114, no. 8, pp. 1827–1849.

[40] KSU-RC. (2007). “KSU-RC: Moment-Curvature, Force and Interaction Analysis of Reinforced Concrete Member, V 1.0.11, Inc.” Kansas State University, Kansas, USA.

[41] Wolf, J. P. (1995). “Cone models as a strength-of-materials approach to foundation vibration.” In Proceedings 10th European Conference on Earthquake

Engineering (No. LCH-CONF-1995-004, pp. 583-592).

[42] Schnabel, P.B., Lysmer, J., Seed, H.B. (1972). "SHAKE: A Computer Program for Earthquake Response Analysis of Horizontally Layered Sites," Report, UCB/EERC-72/12, Univ. of California at Berkeley.

[43] EduPro Civil System, Inc. (1998). ProShake Users Manual – Ground Response Analysis Program, EduPro Civil System, Inc., Redmond, Washington.

[44] ASCE/SEI Seismic Rehabilitation Standards Committee. (2007). "Seismic rehabilitation of existing buildings (ASCE/SEI 41-06)." American Society of Civil Engineers, Reston, VA.

[45] Pacific Earthquake Engineering Research Center (PEER), PEER Next Generation Attenuation (NGA) Database. (2013). https:// ngawest2.berkeley.edu.

[46] Federal Emergency Management Agency. (2005). "Improvement of nonlinear static seismic analysis procedures." FEMA 440, prepared by Applied Technology Council (ATC-55 Project).

[47] Shome, N. (1999). "Probabilistic seismic demand analysis of nonlinear structures." Stanford University.

[48] Ibarra, L. F., Krawinkler, H. (2005). "Global collapse of frame structures under seismic excitations." Berkeley, CA: Pacific Earthquake Engineering Research Center, pp. 29-51.

[49] Zareian, F., Krawinkler, H., Ibarra, L., Lignos, D. (2010). "Basic concepts and performance measures in prediction of collapse of buildings under earthquake ground motions." The Structural Design of Tall and Special Buildings, Vol. 19(1-2), pp. 167-181.